NASA
Technical
Paper
2728

August 1987

Effect of Reynolds Number Variation on Aerodynamics of a Hydrogen-Fueled Transport Concept at Mach 6

Jim A. Penland and
Don C. Marcum, Jr.

NASA
Technical
Paper
2728

1987

Effect of Reynolds Number Variation on Aerodynamics of a Hydrogen-Fueled Transport Concept at Mach 6

Jim A. Penland and
Don C. Marcum, Jr.

Langley Research Center
Hampton, Virginia

National Aeronautics
and Space Administration

**Scientific and Technical
Information Office**

Summary

Two separate tests have been made on the same blended wing-body hydrogen-fueled transport model at a Mach number of about 6 and a range of Reynolds number (based on theoretical body length) of 1.577×10^6 to about 55.36×10^6. The results of these tests, made in a conventional hypersonic blowdown tunnel and a hypersonic shock tunnel, are presented through range of angle of attack from $-1°$ to $8°$, with an extended study at a constant angle of attack of $3°$. The model boundary-layer flow appeared to be predominantly turbulent except for the low Reynolds number shock tunnel tests. Model wall temperatures varied considerably between the two tests; the blowdown tunnel varied from about 255°F to 340°F, whereas the shock tunnel had a constant 70°F model wall temperature. The experimental normal-force coefficients were essentially independent of Reynolds number. A current theoretical computer program was used to study the effect of Reynolds number. Theoretical predictions of normal-force coefficients were good, particularly at anticipated cruise angles of attack, that is, $2°$ to $5°$. Axial-force coefficients were generally underestimated for the turbulent skin friction conditions and pitching-moment coefficients could not be predicted reliably.

Introduction

The interpretation and application of aerodynamic test data from ground test facilities in the determination of full-scale aerodynamic performance of a particular design are the primary goals of configuration testing. These goals are accomplished by selecting a design having sufficient volume to house the required fuel and payload, adequate wing area for a safe landing, and a shape based on available theory, published data, and experience. Such a configuration was the liquid-hydrogen-fueled hypersonic transport concept (fig. 1) that was extensively tested through a wide range of Reynolds number in a conventional blowdown wind tunnel and a shock tunnel at a Mach number of about 8 and reported in references 1 and 2.

The purpose of this paper is to report the results of further free-transition tests on the same model of references 1 and 2 at a lower Mach number of about 6 in both a blowdown tunnel and a shock tunnel.

The major difference existing between tests in the two tunnels was the ratio of model wall temperature to stagnation temperature. The shock tunnel data were taken with a relatively low model wall temperature, whereas the conventional wind-tunnel data were taken with a high model wall temperature.

Presentation of results includes a comparison of all experimental longitudinal force and moment coefficients measured in a conventional blowdown hypersonic tunnel and those measured in a hypersonic shock tunnel; experimental data are then compared with theoretical predictions made with Gentry's Hypersonic Arbitrary-Body Aerodynamics Computer Program (Mark III Version) (GHABAP). (See ref. 3.) The experimental data were obtained at a Mach number of about 6 through a range of Reynolds number (based on theoretical model body length) from about 1.577×10^6 to about 55.36×10^6. The range of angle of attack was from $-1°$ to about $8°$. The results of a study of data at a constant angle of attack of $3°$ are also presented.

Symbols

C_A	axial-force coefficient, $\frac{F_A}{q_\infty S}$
C_D	drag coefficient, $\frac{D}{q_\infty S}$
C_F	average skin friction coefficient
C_L	lift coefficient, $\frac{L}{q_\infty S}$
C_m	pitching-moment coefficient, $\frac{M_Y}{q_\infty S \bar{c}}$
C_N	normal-force coefficient, $\frac{F_N}{q_\infty S}$
c	wing chord
$\bar{c}$	mean aerodynamic chord of total wing
D	drag, $F_N \sin \alpha + F_A \cos \alpha$
F_A	axial force along X-axis (positive direction is $-X$)
F_N	normal force along Z-axis (positive direction is $-Z$)
L	lift, $F_N \cos \alpha - F_A \sin \alpha$
L/D	lift-drag ratio
l	reference length (theoretical body length), 25.92 in. (see fig. 1)
M	free-stream Mach number
M_Y	moment about Y-axis
p_o	stagnation pressure
q_∞	free-stream dynamic pressure
R_l	Reynolds number based on theoretical body length at free-stream conditions

S	reference area, area of wing including fuselage intercept, 70 in^2
S_p	planform area, in^2
T_o	stagnation temperature, °R
V	volume, in^3
α	angle of attack, deg

Subscripts:

LE	leading edge
TE	trailing edge
cl	centerline

Abbreviations:

Exp.	experiment
GHABAP	Gentry's Hypersonic Arbitrary-Body Aerodynamics Program (Mark III Version)
HST	Hypersonic Shock Tunnel
Inv.	inviscid
LRC	Langley Research Center
M = 6 LRC 20"	Langley 20-Inch Mach 6 Tunnel
M = 8 LRC VDT	Langley Mach 8 Variable-Density Tunnel
TC	tangent-cone pressure distribution method
TW	tangent-wedge pressure distribution method
t.p.	tangent point

Fuselage dimensions in table II and figure 2:

A	distance between reference line and top of fuselage
H	height of fuselage
rad. B	radius of fuselage bottom
rad. E	radius of fuselage side
rad. LS	radius of strake lower surface
rad. T	radius of fuselage top
rad. US	radius of strake upper surface
rad. W	radius of fairing from fuselage to wing
Sd	distance from bottom of fuselage to strake leading edge
SW	distance from side of fuselage to strake leading edge
x	distance from nose of fuselage to cross section
x/l	body station

Test Configuration

The test model was the 1/150-scale hypersonic transport concept of references 1 and 2 and is shown in figure 1. The fuselage cross-section design was semielliptical with a width-height ratio of 2 to 1; the cross-sectional area was expanded from the nose to a maximum at the 0.66 body station according to the Sears-Haack volume distribution equations for minimum drag bodies of reference 4 and converged to 0 at station 1.00. Strakes were added to improve the hypersonic lifting capability of this voluminous component. The fuselage was blended with the strakes and the wing to reduce adverse component interference effects. (Details of the configuration tested are shown by the solid lines in fig. 1.) The vertical tail and engine nacelle were not installed for the present tests. The fuselage cross-section design scheme is shown in figure 2. All design curves were circular arcs to facilitate fabrication. The overall geometric characteristics of the model are presented in table I, and the detailed fuselage dimensions illustrated in figure 2 are presented in table II. The model was constructed entirely of 4130 steel to provide maximum strength in an annealed condition. The model fuselage was machined to accept a six-component strain gauge balance to measure aerodynamic forces and moments during the wind-tunnel tests.

Apparatus and Tests

Langley 20-Inch Mach 6 Tunnel

This investigation was conducted in the Langley 20-Inch Mach 6 Tunnel. This tunnel operates on a blowdown cycle through a two-dimensional nozzle with a test section 20.5 in. high and 20 in. wide. Dry air was used for all tests to avoid water condensation effects, and it was heated to avoid air liquefaction and the supersaturated region as defined by reference 5. Tests were conducted at free-stream Mach numbers of 5.799 to 5.994, stagnation pressures of 34.3 to 525 psia, and stagnation temperatures of about 784°R to 912°R. These conditions result in an average free-stream Reynolds number based on body length of 1.577×10^6 to 18.20×10^6 (0.7303×10^6 to 8.426×10^6 per foot).

A six-component water-cooled strain gauge balance was installed inside the model body and was

attached to the tunnel variable angle sting support system. The angle of attack was set for each test point by the reflection of a beam of light from a fixed-point source to a small mirrored prism/lens installed flush with the surface of the model to a calibration board. Thus, by setting the model at the desired angle of attack instead of the sting support, no sting deflection correction was required. Forces and moments were measured through a range of angle of attack from $-1°$ to $8°$ at an angle of sideslip of $0°$. All screw and dowel holes and joints were filled with dental plaster before each test run. Base pressures were measured and the axial-force component was adjusted to correspond to a base pressure equal to the free-stream static pressure. All tests were conducted with natural boundary-layer transition.

Calspan Hypersonic Shock Tunnel

The Calspan 48-inch leg of the Hypersonic Shock Tunnel, described in reference 6, employs a reflected shock to process air to conditions suitable for supplying an axially symmetric convergent-divergent hypersonic nozzle. The shock-processed air is expanded through a contoured nozzle, having interchangeable throats, to the desired test conditions at the 24-inch exit diameter. Test time varied with conditions up to about 13 milliseconds duration. For the shock tunnel tests the stagnation pressure varied from about 259 to 4093 psia, and stagnation temperature varied from about 1479°R to 2289°R to tailor the wide test Reynolds number range at Mach numbers of 6.13 and 6.58 and to avoid liquefaction. These conditions resulted in an average free-stream Reynolds number based on body length of 1.64×10^6 to 55.36×10^6 (0.7599×10^6 to 25.63×10^6 per foot). The higher stagnation temperatures were utilized at the lower stagnation pressures to help obtain the lower Reynolds numbers by increasing viscosity. The model was mounted on a three-component strain gauge balance downstream of the contoured nozzle exit at a fixed angle of attack for all tests, and the final data were corrected for sting deflection. The free-stream Mach number was determined from pitot pressures measured for each test run by means of piezoelectric crystal pressure transducers mounted in the test section. Tests were made with free transition, and base-pressure corrections were applied as described in the previous section on the blowdown tunnel.

Precision of Data

Estimates of the uncertainties in the measurement of force and moment coefficients for the individual test points are generally based on the accuracy of the force balance system, which is ± 0.5 percent of maximum balance loads with all components loaded simultaneously. During the present tests, only the normal-force, axial-force, and pitching-moment components were utilized and the balance was check calibrated at full, one-third, and one-fifteenth loads. Due to these precautions, an accuracy of ± 0.125 percent of full load is considered a more reasonable estimate and is presented as follows for the low Reynolds number worst condition:

C_N	± 0.002
C_A	± 0.0004
C_m	± 0.0002

The stagnation pressure was measured to an accuracy of ± 0.003 to ± 1.3 psia for the pressure range of 35 to 525 psia and the angle of attack was set to $\pm 0.10°$.

Theoretical Methods

The theoretical studies made in the present report consist of, first, computerized calculations predicting the various longitudinal aerodynamic coefficients at appropriate flow conditions for angles of attack up to $8°$ and, second, an investigation of the normal and axial forces with variation in Reynolds number at a constant angle of attack of $3°$. The computer program was also used to evaluate the induced pressure effects on axial-force coefficients under laminar boundary conditions.

Inviscid Aerodynamics

The theoretical studies make major use of Gentry's Hypersonic Arbitrary-Body Aerodynamics Program (Mark III Version) (GHABAP). (See ref. 3.) The aircraft configuration was divided into approximately 800 elements, as shown in figure 3, for the calculation of both the inviscid and viscid aerodynamics. This program has available a variety of optional calculation methods for inviscid pressure versus flow deflection in both the impact flow and the shadow flow regions, which may be arbitrarily applied to individual model panels. Various methods and distributions were tried on the present configuration including the tangent-cone, tangent-wedge, and the shock-expansion methods for the impact flow regions while using the Prandtl-Meyer expansion from free stream to all shadow regions. The most successful combination was found to be the use of the tangent-cone pressure distribution on the forward fuselage and strakes ahead of the wing-fuselage junction and the tangent-wedge method on the wings and that portion of the fuselage aft of the wing-fuselage junction as discussed subsequently. This

distribution methods gave normal- and axial-force coefficients on the complete configuration that were essentially the same as those predicted by the use of the tangent-cone option on the fuselage and the shock-expansion option on the wings and strakes, as presented in reference 1, but gave much more realistic pitching-moment coefficients at $M = 8$ (ref. 2). This compromise in selection of inviscid pressure distribution calculation methods is reasonable when consideration is given to the flattened conical shape of the forward fuselage and to the relatively small average thickness ratio of the aft blended wing-body cross section. Wing and fuselage leading-edge axial-force contributions were assessed from the results of the circular-cylinder study of reference 7. A base pressure coefficient of $-1/M^2$ (ref. 8) was assumed to exist on the blunt-wing trailing edge.

Skin Friction

Laminar skin friction was calculated within the GHABAP by the T'-theory (the reference temperature method of Monaghan in ref. 9). A discussion of this reference temperature calculation was presented in reference 2.

Turbulent skin friction was calculated within the GHABAP by the method of Spalding and Chi (ref. 10). Adiabatic wall temperature was assumed for both laminar and turbulent calculations of viscous effects for the Mach 6 blowdown tunnel tests. For the shock tunnel estimates, the measured wall temperature of 70°F (530°R) was used.

Induced Pressure

The buildup of a boundary layer on an aerodynamic surface effectively alters the surface contour; consequently, the resulting airflow is displaced outward from the surface which changes the pressure distribution. The boundary layer of some of the present tests was laminar, and due to the effective surface contour changes and additional effective blunting of the leading edges, there were marked local flow deflections and, therefore, high local pressures, which decreased rapidly downstream to levels somewhat higher than would be expected for inviscid flow. (See refs. 2 and 11.) To account for this change in surface pressures on both wings and body, the induced pressure option available in the GHABAP was used to provide estimates for comparisons between theory and experiment with angle of attack. It is generally recognized that turbulent boundary layers are equally capable of inducing surface pressure changes but little experimental effort has been made to understand this important phenomenon. References 12 and 13 are some examples of comparison between theory and experiment under laminar, transitional, and turbulent conditions. No configuration aerodynamics program incorporates pressure effects induced by boundary layers at this time, and no estimates were made for the present tests.

Blunted leading edges of the model may also be expected to induce surface pressure variations; however, no estimates were made for the 0.003-inch-radius leading edges or nose radius of the present test model. (See ref. 11.)

Viscous Interaction

The large induced pressure gradient (falling pressures) discussed in the preceding section has an adverse effect on the laminar skin friction and is hereafter referred to as "viscous interaction." As with the induced pressure calculations, the GHABAP was utilized to account for this viscous interaction. This aerodynamic program normally tabulates the laminar skin friction in combination with an estimate of the viscous interaction. For the present analysis, this program was modified to tabulate the skin friction without the viscous-interaction increment. The increment of viscous interaction was therefore the difference between the original and the modified computer program results. These increments were used in combination with the induced pressure increment and the leading-edge and trailing-edge drag. No estimates of the viscous interaction were made for turbulent boundary-layer conditions.

Results and Discussion

Experimental results at Mach 6 for seven different Reynolds number tests through a range of angle of attack from $-1°$ to $8°$ from a conventional blowdown wind tunnel and a shock tunnel are presented in figures 4 and 5 for the wing-body hypersonic concept and compared with theoretical estimates from the GHABAP. Numerous tests were made at $\alpha = 3°$ through a range of Reynolds number from 1.577×10^6 to 18.199×10^6 in the blowdown tunnel, and two tests were made in the shock tunnel at $R_l = 1.906 \times 10^6$ and 52.963×10^6. These data are presented in figures 6 and 7, along with GHABAP estimates.

Normal Force

Experimental normal-force coefficients, presented against angle of attack in figure 4(a), show only a slight variation between facilities and Reynolds numbers. The largest variation occurred for the shock tunnel cold wall test at low Reynolds number. Each cold wall data point was the result of a separate shock tunnel test made during a period of several days on the same model; this may have contributed

to the data scatter. The change in the slope of the normal-force curve with Reynolds number was due in part to the variation of tunnel test Mach numbers with stagnation pressure. It is evident that the wide range of model surface temperature and stagnation temperature between the blowdown and shock tunnels had only minimal effect on the normal force. The GHABAP estimates are good at cruise angles of attack (2° to 5°) and adequate at higher angles of attack.

Axial Force

The axial-force coefficients from both the blowdown and shock tunnel tests are shown in figure 4(b) and are compared with theoretical estimates computed with the GHABAP. See the section "Theoretical Methods" for a description of the present application of turbulent and laminar skin friction and reference 2 for a detailed discussion of the effects of model wall temperature on the axial force. A study of the left side of figure 4(b) shows that the experimental data taken in the conventional blowdown tunnel with hot model wall temperatures were generally underpredicted by the GHABAP, particularly at the lower angles of attack. For these predictions a turbulent skin friction was assumed although laminar-boundary-layer conditions would be expected to exist at the lower Reynolds numbers. This apparent early transition is discussed subsequently. The present turbulent skin friction estimates do not contain either induced pressure or viscous interaction increments as included in the laminar estimates. (See section "Theoretical Methods.") Furthermore, it is not known with what accuracy the inviscid axial-force coefficients were calculated by the GHABAP. In reference 2, the predicted inviscid axial-force coefficients at $\alpha = 3°$ were substantiated by extrapolation of experimental data taken at low Reynolds number test conditions to very high Reynolds numbers. Such an extrapolation can only be done under laminar conditions where the skin friction parameters are proportional to (Reynolds number)$^{1/2}$. The turbulent skin friction parameter may also be considered to be proportional to (Reynolds number)^{n} but in turn n varies with Reynolds number, thus making simple extrapolation over wide ranges of Reynolds number unreliable if not impossible (ref. 14). It should be pointed out that the turbulent skin friction varies much more with Mach number than does the laminar skin friction; therefore, this contributes to the less than desirable accuracy in predicting configuration axial force with codes that do not take into account local Mach number variations.

The right side of figure 4(b) shows the two available angle-of-attack sweeps from the shock tunnel at widely different Reynolds numbers. Correlation with the GHABAP shows that the lower Reynolds number data may be considered to have been taken with a laminar boundary layer and the higher Reynolds number data with a predominantly turbulent boundary layer. The accuracy of prediction of axial-force coefficients for shock tunnel conditions was superior to those for the blowdown tunnel due in part to the knowledge of the precise model wall temperature. At Reynolds numbers of the order of 10^7 and above, the Spalding and Chi turbulent skin friction predictions are subject to considerable variation with wall temperature. This variation is sufficient to bring the theoretical estimates up to the experimental points at the higher angles of attack for the blowdown tunnel data at $R_l = 18.45 \times 10^6$ (fig. 4(b)) if the unrealistic low wall temperature of 80°F is assumed (ref. 10).

Lift

The lift coefficients for the present wing-body concept are presented in figure 4(c) with GHABAP estimates. Little difference may be seen between Reynolds numbers in the same test facility and/or between facilities except at the highest shock tunnel Reynolds number. Predictions by the GHABAP tend to overpredict the lift, particularly at the higher angles of attack. This overprediction is partially because of the inability of the program to accurately account for the effective airfoil geometry changes due to boundary-layer buildup. Two-dimensional calculations have shown that the addition of displacement boundary-layer contours to a wedge-slab-wedge airfoil will not only increase the pressure axial force and augment the skin friction but will slightly reduce the normal force. Both of these forces contribute to a decrease in lift coefficient at a given angle of attack, which results in a lower lift-curve slope.

Drag

Comparisons of experimental drag coefficients and estimates by the GHABAP are presented in figure 4(d) for all test Reynolds numbers. Because drag is a combination of normal force and axial force and the prediction of normal force was superior to axial force, the difference between theory and experiment was due primarily to the errors in the axial-force prediction. The shock tunnel results were better predicted than the blowdown tunnel results, particularly at the lower angles of attack.

Lift-Drag Ratio

The lift-drag ratios for all tests are presented in figure 4(e) plotted against angle of attack. All estimates by the GHABAP were higher than the experimental data except the turbulent estimate for

the shock tunnel test at the lower Reynolds number. This overprediction is again primarily due to the inaccurate axial-force predictions that, in turn, were due to a variety of reasons discussed previously, including the lack of knowledge of the model wall temperature distribution, the assumption within the computer program that the flow on the model is always streamwise for pressure calculations and longitudinal on the model with no cross flow for skin friction estimates, and inadequate estimates of induced pressure effects. Also, local areas of transition and/or separation were not taken into account by the present computer program.

Pitching Moment

Pitching moments are presented in figure 4(f) for the various Reynolds numbers. The experimental data exhibited a degree of stability at angles of attack up to about 4° where the configuration became neutrally stable and then showed a slight pitch-up at the highest test angles of attack. The theoretical estimates by GHABAP underpredicted the experiment at all angles of attack but did predict the correct slope at the lower angles of attack. Additional experimental testing will be required to determine the reason for the undesirable change in the slope of the pitching-moment curve with angle of attack. As mentioned in the section "Theoretical Methods," the results obtained from the GHABAP are a function of which options for pressure versus flow deflection were selected. Presented in figure 5 are experimental pitching-moment data at various Mach numbers on the present wing-body configuration compared with inviscid estimates from the GHABAP using two different pressure versus flow deflection options. The upper portion of figure 5 shows the results of pitching-moment calculations with the tangent-cone option on the fuselage and the shock-expansion option on the wings and strakes, and the bottom portion of figure 5 shows the tangent-cone option on the forward fuselage and strakes and the tangent-wedge option on the wings and aft fuselage. For Mach 6 the tangent-cone/shock-expansion option used in reference 1 overpredicted the experimental data about as much as the tangent-cone/tangent-wedge (TC/TW) option underpredicted it. The TC/TW option was superior at $M = 8$ and was used in both reference 2 and the present report. The inset plan views show the regions of the model, both upper and lower surfaces, covered by the respective pressure distribution options.

It may be concluded that the tailoring of a specific pressure distribution option scheme in the GHABAP can make possible the reasonable prediction of pitching moments on a specific model under a given set of flow conditions, but no assurance can be assumed for the same model under another set of flow conditions.

The GHABAP estimates, however, do show that the pitch stability is reduced with increasing Mach number. The present experimental data indicate that the change in pitching moment with Mach number is less than predicted. Reference 15 shows similar stability results on the delta-wing X-15 concept tested in the same wind tunnels from which the data in figure 5 were obtained. Additional experimental data at Mach numbers up to 6 may be found in reference 16, along with theoretical estimates, on a similar hypersonic cruise concept. These data were obtained on a larger cast aluminum model with less dimensional accuracy than the present machined model.

Comparison of Experiment and Theory at a Constant Angle of Attack

In parallel with the study carried out in reference 2, a series of tests was carried out at a constant angle of attack of 3° through the widest possible range of Reynolds number in the Langley 20-Inch Mach 6 Tunnel. Two data points were also available from the Calspan Hypersonic Shock Tunnel at $M = 6.13$ and 6.58.

The normal-force and axial-force coefficients from these tests are presented in figure 6 and compared with theoretical estimates utilizing both laminar and turbulent skin friction generated by the GHABAP. The normal-force coefficient is essentially independent of Reynolds number, a conclusion also determined at $M = 8$ in reference 2. The small decrease in normal-force coefficient with Reynolds number was due to the increase in test Mach number with stagnation pressure. The effect of Reynolds number reductions is primarily one of the thickening of the boundary layer. As boundary layers tend to effectively alter the surface contours of the configuration, there is an accompanying variation in the surface pressures. These surface pressure variations always increase the axial force but show minimal effect on normal force at low angles of attack because pressures are induced on both upper and lower surfaces. Excellent predictions of the normal-force coefficients on the wing-body configuration with Reynolds number by the GHABAP are shown. The tangent-cone/tangent-wedge pressure distribution options as illustrated in figure 5 were used for these estimates. The tangent-cone/shock-expansion options produced slightly lower normal-force coefficients.

As the Reynolds number was reduced during these tests, the aerodynamic forces were also reduced because of the decrease in dynamic pressure, which is a function of both the stagnation pressure and the

measured average Mach number. Plots of the tunnel parameters for the tests at $\alpha = 3°$ in the Langley 20-Inch Mach 6 Tunnel are shown in figure 8. The Mach numbers shown were derived from the stagnation pressures shown and a pitot pressure taken prior to the force balance measurements for each data point. The pitot probe was located in the test section at a point determined by wide range calibrations to give an average Mach number at all tunnel stagnation pressures (ref. 17). Thus, there was about a 0.23 variation in Mach number from the lowest to the highest Reynolds number, which corresponded to about an 8-percent change in dynamic pressure caused by Mach number variations alone. It is worth noting that the scatter in the measured Mach numbers with Reynolds number is greater than in the normal-force coefficients, which are sensitive to not only Mach number but to the accuracy of the measurement of pressures and of the setting of the angle of attack. This imparts additional confidence that the Mach number measurement was accurate and that the independence of normal-force coefficient with Reynolds number is a valid conclusion. These observations indicate that the use of a standardized model of known aerodynamic characteristics with Mach number might be used for wind-tunnel calibration where the average Mach number is desired and time is unavailable for customary lengthy pitot pressure distribution measurements and integration procedures.

The axial-force coefficient at a constant angle of attack of 3° is shown in the bottom plot of figure 6. Theoretical estimates using the GHABAP are presented for comparison with the experimental data. Estimates were made for the inviscid axial-force coefficient which decreases slightly with Reynolds number only because the tunnel average Mach number increased as the stagnation pressure was increased to make possible tests at higher Reynolds numbers. The increments in axial-force coefficient due to the wing leading and trailing edges were made as described in the section "Theoretical Methods." The curves for total laminar theory are the sum of the inviscid, leading- and trailing-edge increments and the GHABAP estimates of laminar skin friction, induced pressure, and viscous interaction. A comparison of these program-generated laminar parameters and a more precise but laborious method may be found in reference 2. The curves for total turbulent theory are the sum of the inviscid, leading- and trailing-edge increments, and GHABAP estimates of turbulent skin friction by the Spalding and Chi method.

A comparison of experimental axial-force coefficients at $\alpha = 3°$ with the theoretical estimates in figure 6 indicates that the Mach 6 tunnel data were recorded on a model that was experiencing a predominance of turbulent-boundary-layer flow. The single data point at $\alpha = 3°$ from the Calspan shock tunnel at a low Reynolds number appears to have been recorded with a predominance of laminar flow. The data point at a high Reynolds number from the Calspan tests, on the other hand, appears to have experienced turbulent flow. With the exception of the data point at a high Reynolds number from Calspan, all data were underpredicted. Part of this underprediction may well be an inaccurate estimate of the inviscid axial-force coefficient at $\alpha = 3°$. As previously discussed, there is no way that this estimate can be substantiated. The lack of induced pressure and viscous interaction estimates for the turbulent estimates and the simplified program estimates for the laminar estimates could also contribute to the underpredictions.

The apparent early transition that occurred on the model during tests in the Langley 20-Inch Mach 6 Tunnel is a subject for future study and present speculation. It is known that the transition Reynolds number can be decreased by a variety of phenomena including

Tunnel noise emanating from wall boundary layer
Tunnel noise emanating from upstream turbulence in settling chamber
Tunnel size decrease
Tunnel wall temperature increase
Model wall temperature increase
Unit Reynolds number decrease in given tunnel
Mach number decrease above $M \approx 3$
Leading-edge sweep increase
Leading-edge and nose-diameter decrease
Tests in the $M = 1$ to 3 region
Surface roughness

Detailed discussions of transition at hypersonic speeds may be found in references 17 to 23. It is not known how many of these or other more obscure transition factors affected the present blowdown tunnel data. Further, different Reynolds number tests on configuration-type models in a variety of facilities may be needed to resolve the question. The resulting lift, drag, and lift-drag ratio obtained by resolving the normal and axial forces of figure 6 at an angle of attack of 3° are presented in figure 7. The estimates of lift and drag coefficients by the GHABAP follow the same trends as did the predictions of normal- and axial-force coefficients in figure 6. The prediction of lift-drag ratio tends to smooth out the variations between the experiment and theory such that the

overpredictions for the blowdown tunnel hot wall tests varied only from about 4 to 5 percent, and variations for the Calspan cold wall tests were somewhat less.

Conclusions

An analysis of experimental data for a hydrogen-fueled, blended wing-body hypersonic transport concept from a conventional wind tunnel and a shock tunnel at a Mach number of about 6 through a range of Reynolds number (based on fuselage theoretical length) from 1.577×10^6 to about 55.36×10^6 leads to the following conclusions:

1. There were only slight variations of normal-force coefficients with Reynolds number through an angle-of-attack range of $-1°$ to $8°$ in the blowdown tunnel with hot model wall conditions.

2. Gentry's Hypersonic Arbitrary-Body Aerodynamics Program (Mark III Version) (GHABAP) provided good theoretical predictions of the normal-force coefficients with angle of attack and with Reynolds number, particularly at anticipated cruise angles of attack, that is, $2°$ to $5°$.

3. All tests conducted in the Langley 20-Inch Mach 6 Tunnel and the high Reynolds number test in the Calspan Hypersonic Shock Tunnel appeared to have been made with predominantly turbulent boundary-layer conditions.

4. The accuracy of the GHABAP estimates of the inviscid axial-force coefficients could not be determined.

5. The GHABAP underestimated all axial-force data at low angles of attack when turbulent skin friction was assumed, except for the high Reynolds number cold wall shock tunnel data.

6. The GHABAP underestimated the axial-force coefficients of the low Reynolds number cold wall Calspan test while using laminar skin friction, plus the induced pressure and viscous interaction options.

7. Pitching-moment coefficients cannot be predicted reliably with the present GHABAP methods, although the program does predict the trends with Mach number.

NASA Langley Research Center
Hampton, Virginia 23665-5225
June 18, 1987

References

1. Penland, J. A.; and Romeo, D. J.: Advances in Hypersonic Exploration Capability—Wind Tunnel to Flight Reynolds Number. *J. Aircr.*, vol. 8, no. 11, Nov. 1971, pp. 881–884.
2. Penland, Jim A.; Marcum, Don C., Jr.; and Stack, Sharon H.: *Wall-Temperature Effects on the Aerodynamics of a Hydrogen-Fueled Transport Concept in Mach 8 Blowdown and Shock Tunnels.* NASA TP-2159, 1983.
3. Gentry, Arvel E.: *Hypersonic Arbitrary-Body Aerodynamic Computer Program (Mark III Version). Volume I—User's Manual.* Rep. DAC 61552, Vol. I (Air Force Contract Nos. F33615 67 C 1008 and F33651 67 C 1602), McDonnell Douglas Corp., Apr. 1968. (Available from DTIC as AD 851 811.)
4. Sears, William R.: On Projectiles of Minimum Wave Drag. *Q. Appl. Math.*, vol. IV, no. 4, Jan. 1947, pp. 361–366.
5. Daum, Fred L.; and Gyarmathy, George: Condensation of Air and Nitrogen in Hypersonic Wind Tunnels. *AIAA J.*, vol. 6, no. 3, Mar. 1968, pp. 458–465.
6. *Hypersonic Shock Tunnel—Description and Capabilities.* Calspan Corp., Sept. 1975.
7. Penland, Jim A.: *Aerodynamic Characteristics of a Circular Cylinder at Mach Number 6.86 and Angles of Attack up to 90°.* NACA TN 3861, 1957. (Supersedes NACA RM L54A14.)
8. Mayer, John P.: *A Limit Pressure Coefficient and an Estimation of Limit Forces on Airfoils at Supersonic Speeds.* NACA RM L8F23, 1948.
9. Monaghan, R. J.: *An Approximate Solution of the Compressible Laminar Boundary Layer on a Flat Plate.* R. & M. No. 2760, British Aeronautical Research Council, 1953.
10. Spalding, D. B.; and Chi, S. W.: The Drag of a Compressible Turbulent Boundary Layer on a Smooth Flat Plate With and Without Heat Transfer. *J. Fluid Mech.*, vol. 18, pt. 1, Jan. 1964, pp. 117–143.
11. Bertram, Mitchel H.: Viscous and Leading-Edge Thickness Effects on the Pressures on the Surface of a Flat Plate in Hypersonic Flow. *J. Aeronaut. Sci.*, vol. 21, no. 6, June 1954, pp. 430–431.
12. Stollery, J. L.; and Bates, L.: Turbulent Hypersonic Viscous Interaction. *J. Fluid Mech.*, vol. 63, pt. 1, Mar. 18, 1974, pp. 145–156.
13. Watson, Ralph D.: *Characteristics of Mach 10 Transitional and Turbulent Boundary Layers.* NASA TP-1243, 1978.
14. Bertram, Mitchel H.: *Calculations of Compressible Average Turbulent Skin Friction.* NASA TR R-123, 1962.
15. Goldberg, Theodore J.; Hefner, Jerry N.; and Stone, David R.: *Hypersonic Aerodynamic Characteristics of Two Delta-Wing X-15 Airplane Configurations.* NASA TN D-5498, 1969.
16. Ellison, James C.: *Investigation of the Aerodynamic Characteristics of a Hypersonic Transport Model at Mach Numbers to 6.* NASA TN D-6191, 1971.
17. Goldberg, Theodore J.; and Hefner, Jerry N. (appendix by James C. Emery): *Starting Phenomena for Hypersonic Inlets With Thick Turbulent Boundary Layers at Mach 6.* NASA TN D-6280, 1971.
18. Stainback, P. Calvin (appendix by P. Calvin Stainback and Kathleen C. Wicker): *Effect of Unit Reynolds Number, Nose Bluntness, Angle of Attack, and Roughness on*

Transition on a 5° Half-Angle Cone at Mach 8. NASA TN D-4961, 1969.

19. Hopkins, Edward J.; Jillie, Don W.; and Sorensen, Virginia L.: *Charts for Estimating Boundary-Layer Transition on Flat Plates.* NASA TN D-5846, 1970.
20. Cary, Aubrey M., Jr.: *Turbulent-Boundary-Layer Heat-Transfer and Transition Measurements With Surface Cooling at Mach 6.* NASA TN D-5863, 1970.
21. Stainback, P. Calvin; Wagner, Richard D.; Owen, F. Kevin; and Horstman, Clifford C.: *Experimental Studies of Hypersonic Boundary-Layer Transition and Effects of Wind-Tunnel Disturbances.* NASA TN D-7453, 1974.
22. Ashby, George C., Jr.; and Harris, Julius E.: *Boundary-Layer Transition and Displacement-Thickness Effects on Zero-Lift Drag of a Series of Power-Law Bodies at Mach 6.* NASA TN D-7723, 1974.
23. Pate, Samuel R.: Effects of Wind Tunnel Disturbances on Boundary-Layer Transition With Emphasis on Radiated Noise: A Review. AIAA-80-0431, Mar. 1980.

Table I. Geometric Characteristics of Model

Wing:	
Reference area (includes area projected to fuselage centerline), in^2	70.00
Exposed area outboard of strakes, in^2	30.23
Wetted area, in^2	60.42
Span, in.	9.730
Aspect ratio	1.353
Root chord (on fuselage centerline), in.	13.086
Tip chord, in.	1.308
Taper ratio	0.099
Mean aerodynamic chord of total wing, in.	8.810
Sweepback angle, deg of—	
Leading edge	65.0
25-percent chord line	56.99
Trailing edge	−15.4
Dihedral angle (airfoil mean line), deg	0
Incidence angle, deg	0
Thickness ratio of wing airfoil section (see fig. 1) at —	
Exposed root	0.03
Tip	0.03
Leading-edge radius, in., at —	
Fuselage centerline chord	0.003
Tip	0.003
Trailing-edge height	0.006
Center fin proposed (vertical tail):	
Area (exposed), in^2	12.399
Span (exposed), in.	3.672
Aspect ratio of exposed area	1.09
Root chord (fuselage surface line), in.	5.353
Tip chord, in.	1.390
Taper ratio	0.259
Mean aerodynamic chord of exposed area, in.	3.759
Sweepback angle, deg, of —	
Leading edge	60
Trailing edge	−30
Thickness ratio of fin airfoil section at —	
Tip	0.06
Root	0.06
Leading-edge radius, in.	0.003
Fuselage:	
Length of theoretical model, in.	25.92
Length of test model, in.	23.61
Maximum height, in.	1.428
Maximum width excluding strakes, in.	2.856
Nose radius, in.	0.003
Fineness ratio of equivalent round body (excluding strakes)	13.0

Base area, in^2	1.710
Complete model (excluding vertical tail and engine):	
Planform area of theoretical model, in^2	100.541
Planform area of test model, in^2	98.268
Aspect ratio of theoretical-model planform	0.942
Aspect ratio of test-model planform	0.963
Wetted area, approximate, in^2	225.0
Model scramjet engine (proposed):	
Frontal area, 2 percent wing area, in^2	1.40
Chord ratio of width to height	4.8
Volume of test model, in^3	54.70
$V^{2/3}/S_p$ (test model)	0.146

Table II. Cross-Sectional Dimensions of Fuselage

[All values are in inches]

x/l	x	H	A	rad. B	rad. T	rad. US	rad. LS	rad. E	Sd	SW	rad. W
0	0	0	0.396	0	0	0	0	0	0	0	
.067	1.728	.411	.194	1.508	.465	.084	.632	.103	.101	.084	
.133	3.456	.663	.083	2.436	.752	.389	1.264	.166	.163	.154	
.200	5.184	.862	.025	3.164	.977	.457	1.897	.216	.212	.216	
.267	6.912	1.022	0	3.751	1.158	.533	2.529	.255	.251	.274	
.333	8.639	1.151	0	4.233	1.304	.547	3.161	.288	.283	.332	
.400	10.368	1.253	0	4.597	1.419	.590	3.791	.313	.308	.383	
.467	12.096	1.316	0	4.828	1.491	.644	4.424	.329	.324	.429	
.533	13.824	1.379	0	5.058	1.562	.634	5.058	.345	.339	.465	
.600	15.552	1.426	0	5.234	1.616	[a].522	5.234	.357	.353	[b]1.014	1.440
.667	17.279	1.428	0	5.242	1.618	[a].392		.357	.351	[b]1.819	3.870
.700	18.144	1.426	0	5.234	1.616	[a].389		.356	.342	[b]2.224	4.320
.733	19.008	1.378	.007	5.058	1.562	[a].432		.345	.313	[b]2.676	1.800
.767	19.872	1.316	.032	4.828	1.491	[a].457		.329	.281	[b]3.141	1.080
.800	20.736	1.253	.076	4.597	1.419	[a].529		.313	.245	[b]3.607	1.800
.833	21.599	1.151	.126	4.223	1.304	[a].601		.288	.198	[b]3.174	2.016
.867	22.464	1.022	.180	3.751	1.158	0		.256	.117	2.485	2.808
.900	23.328	.862	.230	3.164	.977			.216			
.933	24.192	.663	.284	2.436	.752			.166			
.967	25.056	.411	.338	1.508	.465			.103			
1.000	25.920	0	.396	0	0			0			

[a]Fairing to wing.

[b]Distance to leading edge or tip.

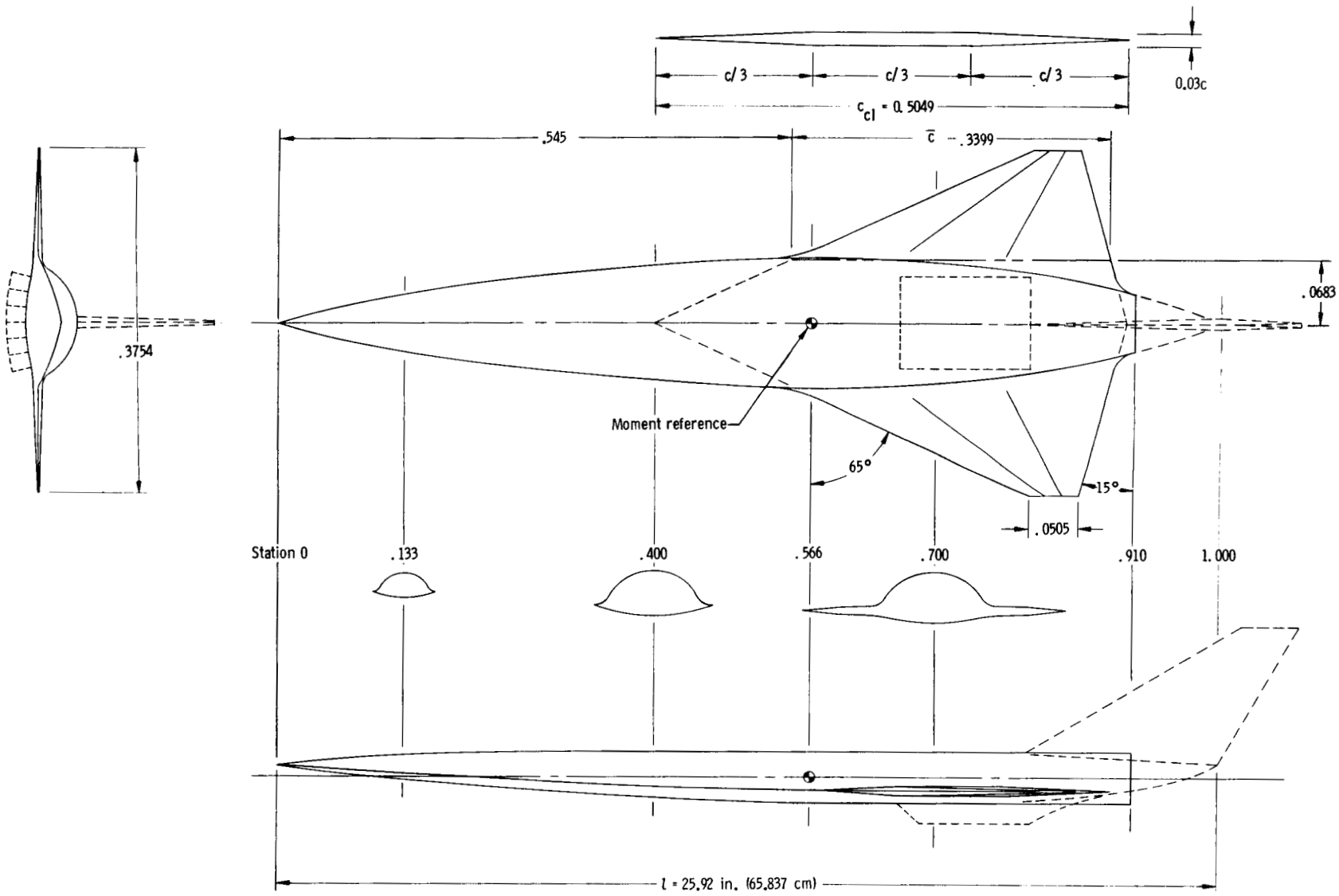

Figure 1. Details of wind-tunnel model. All dimensions have been normalized by the fuselage theoretical length, $l = 25.92$ in., dashed lines show components not in present test.

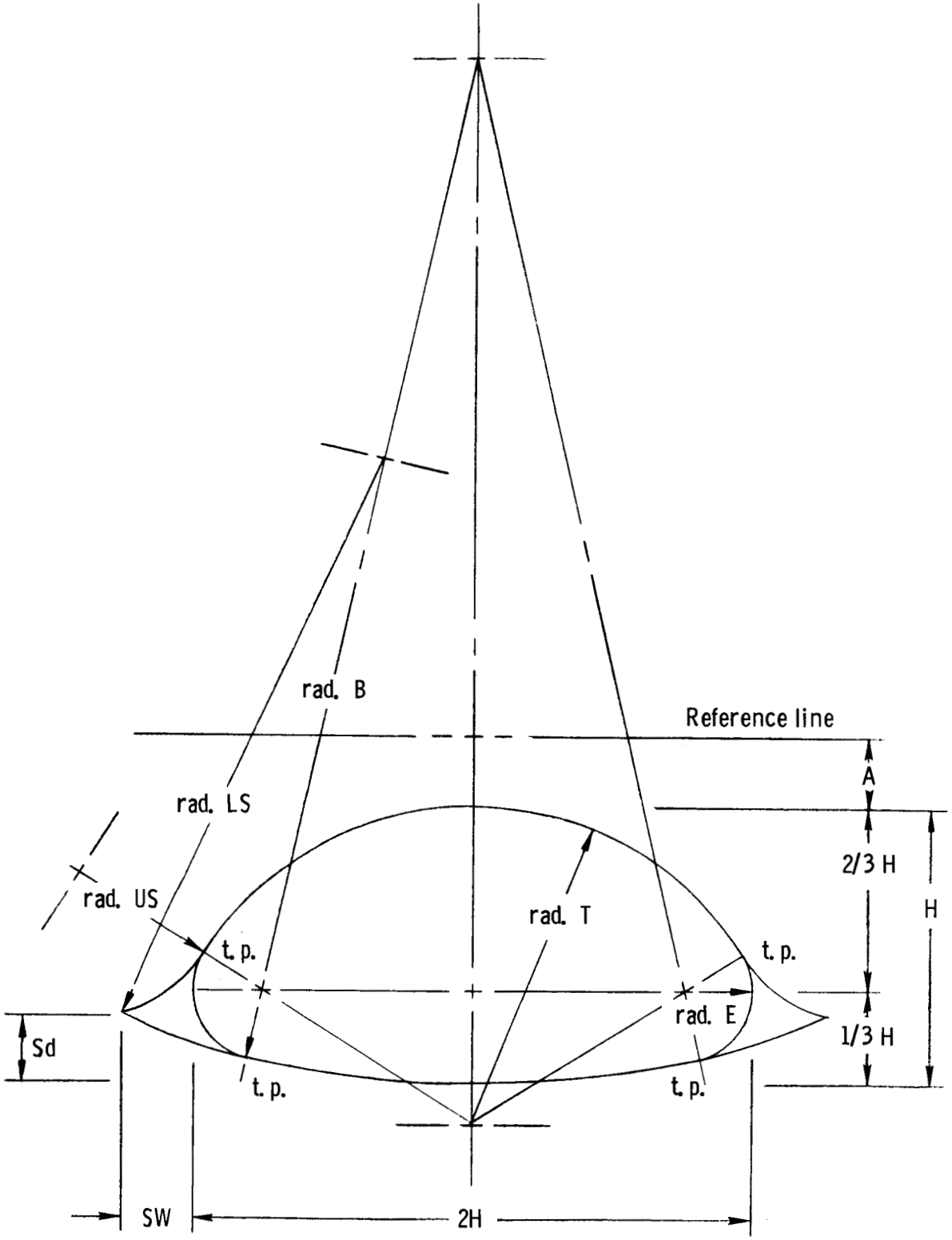

Figure 2. Detail of fuselage cross section and strake design. Dimensions are listed in table II.

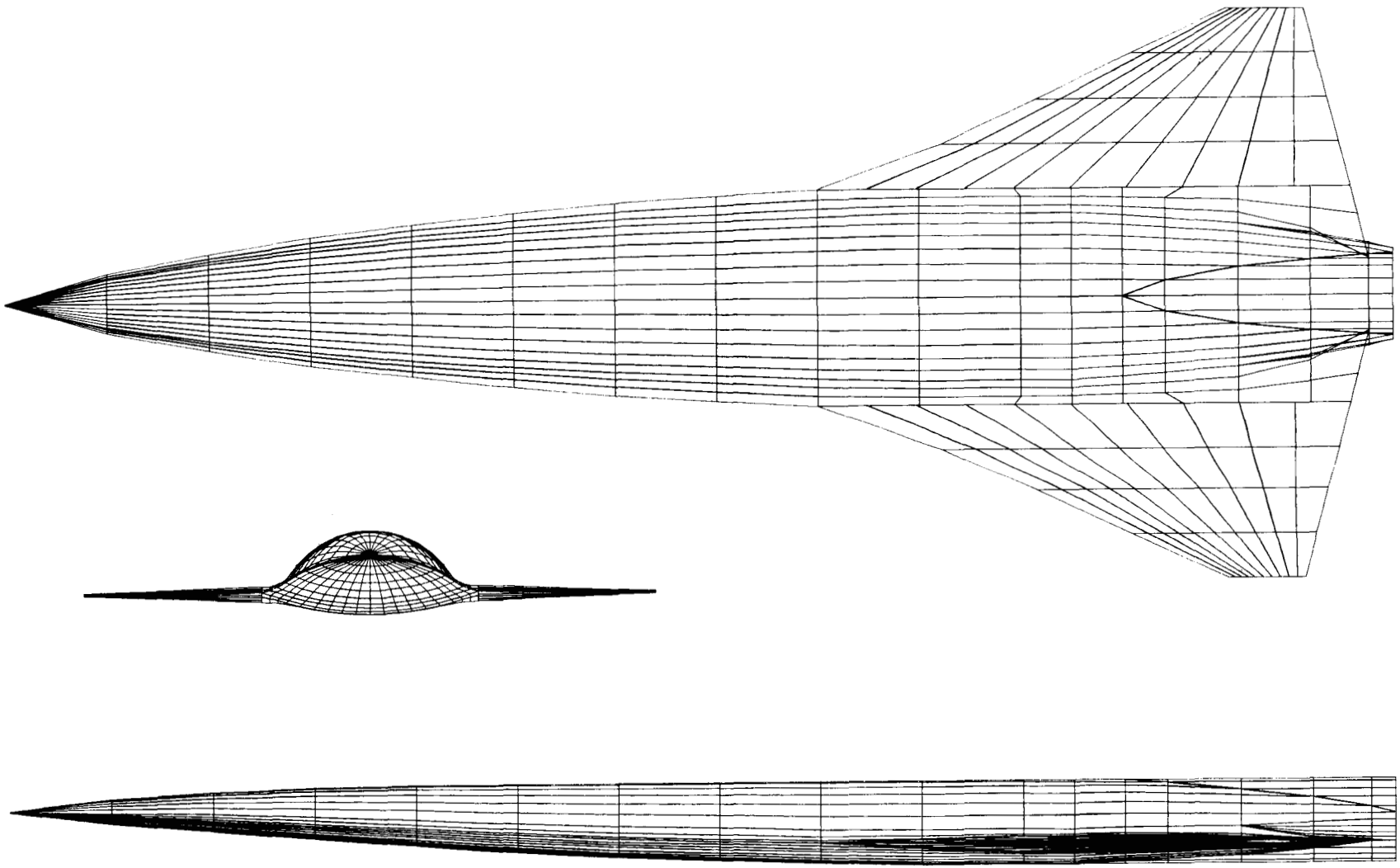

Figure 3. Computer drawing of paneling scheme of configuration as input for hypersonic aerodynamic calculations.

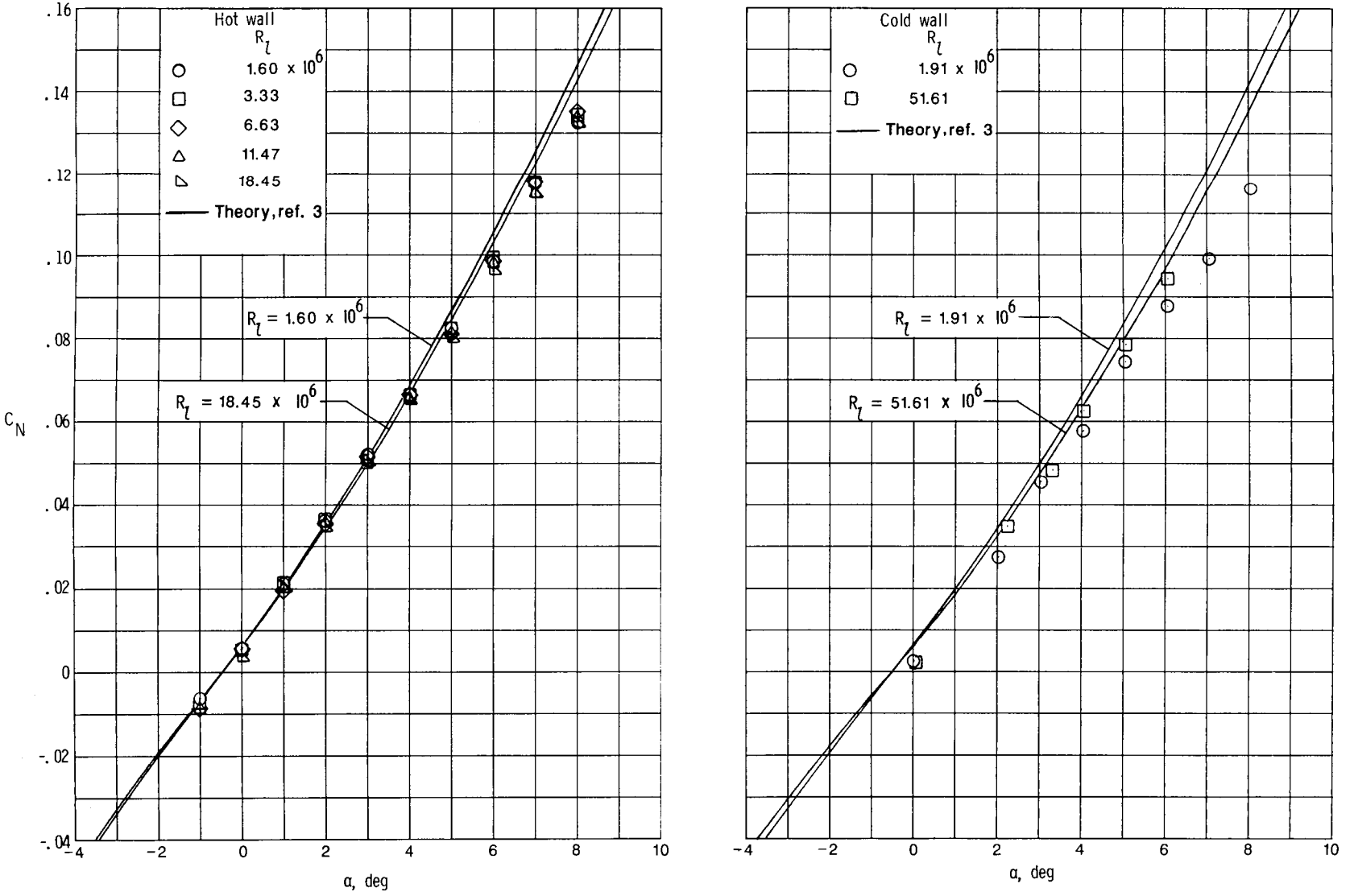

(a) Normal force.

Figure 4. Comparison of theoretical force and moment coefficients with experimental data for various Reynolds numbers in Langley 20-Inch Mach 6 Tunnel (hot wall) and Calspan Hypersonic Shock Tunnel (cold wall).

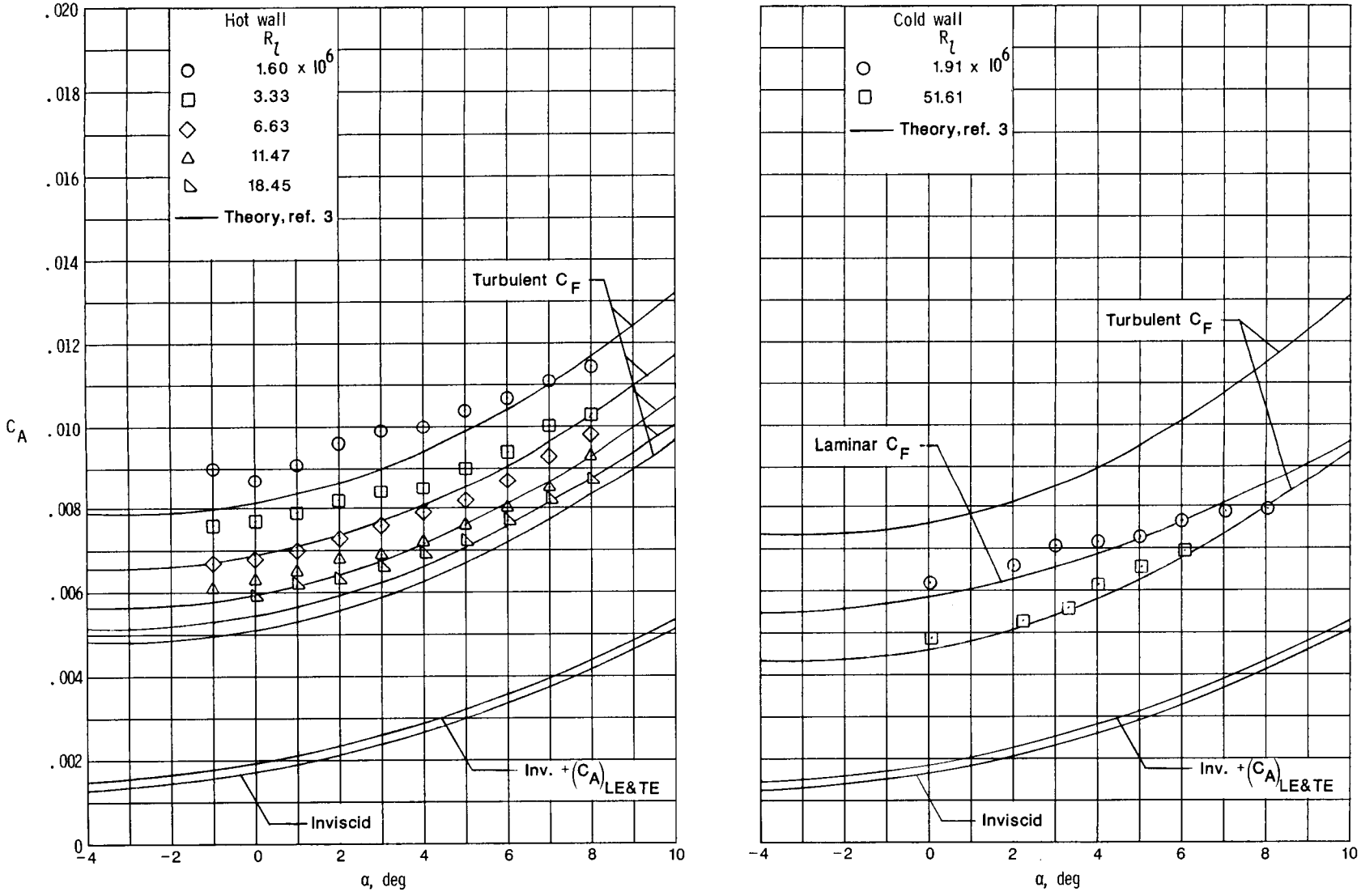

(b) Axial force.

Figure 4. Continued.

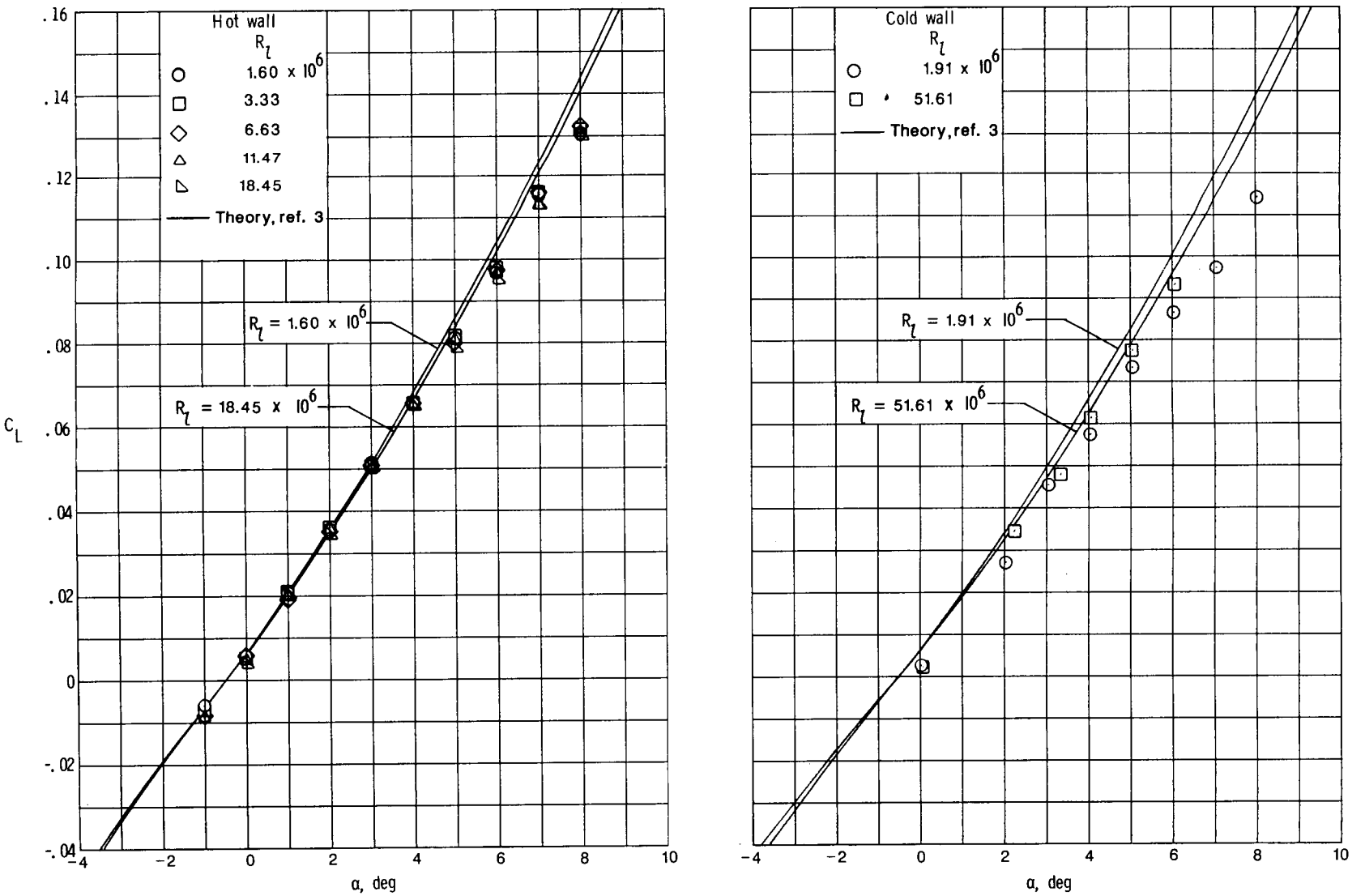

(c) Lift.

Figure 4. Continued.

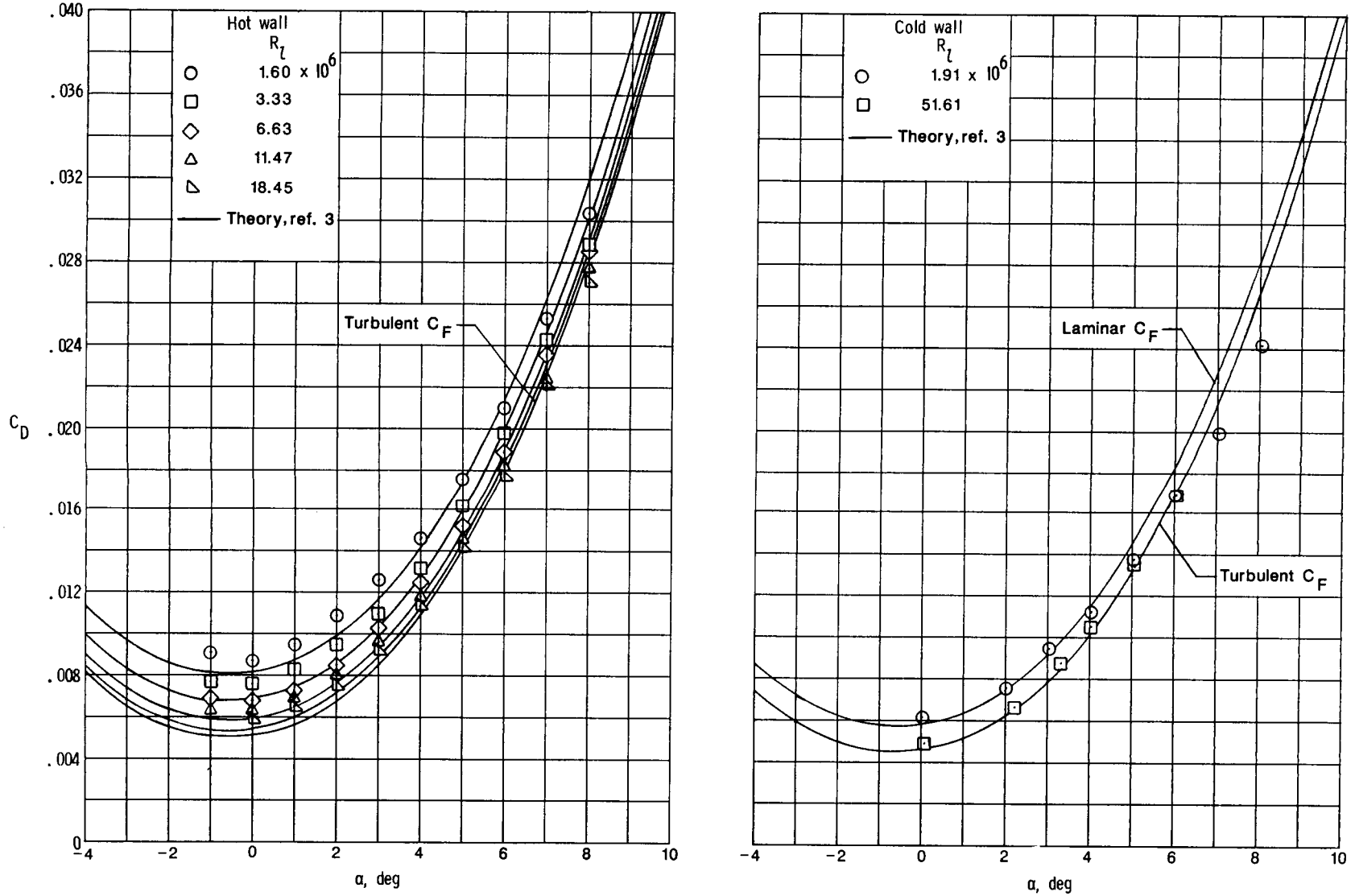

(d) Drag.

Figure 4. Continued.

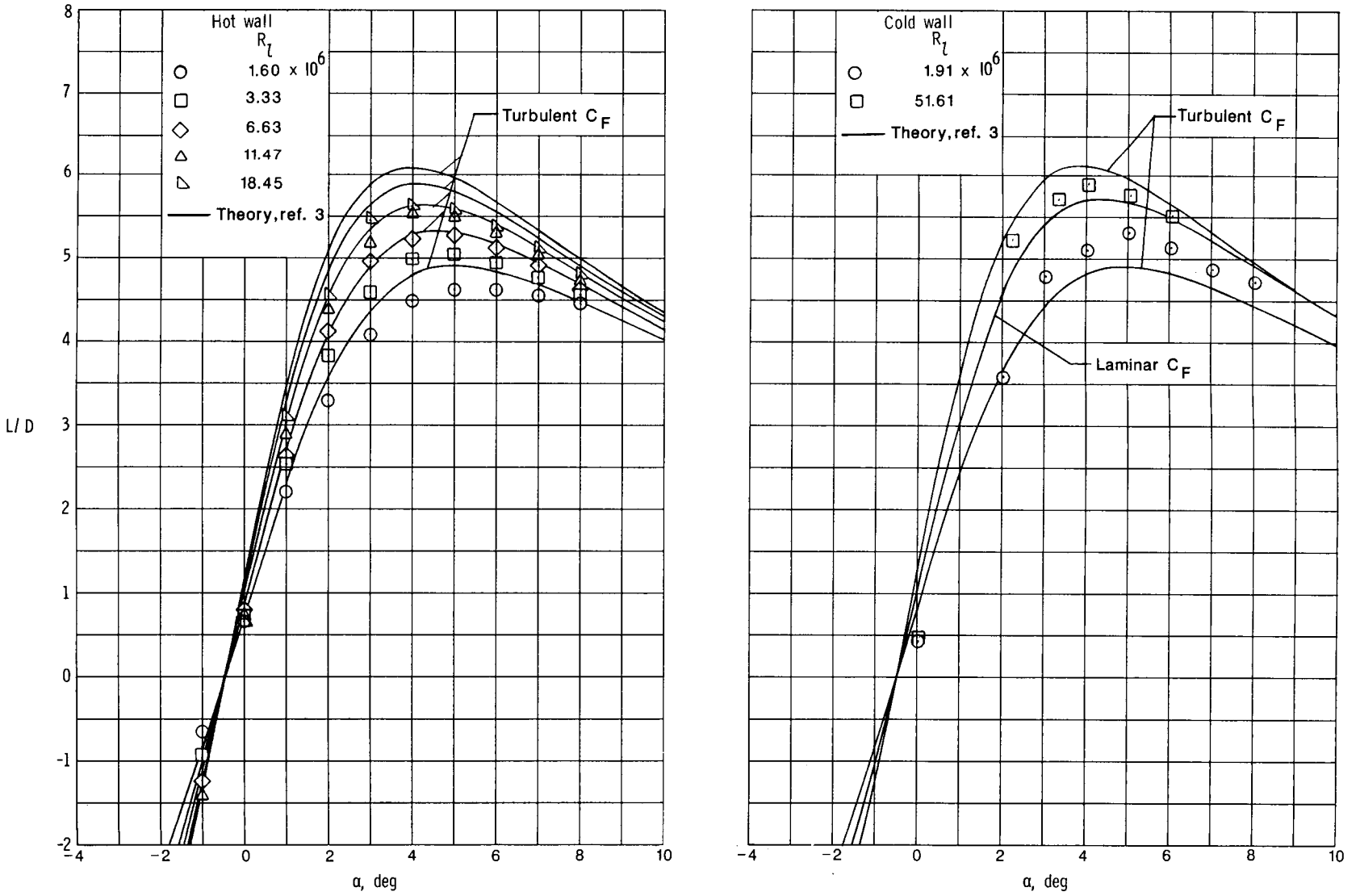

(e) Lift-drag ratio.

Figure 4. Continued.

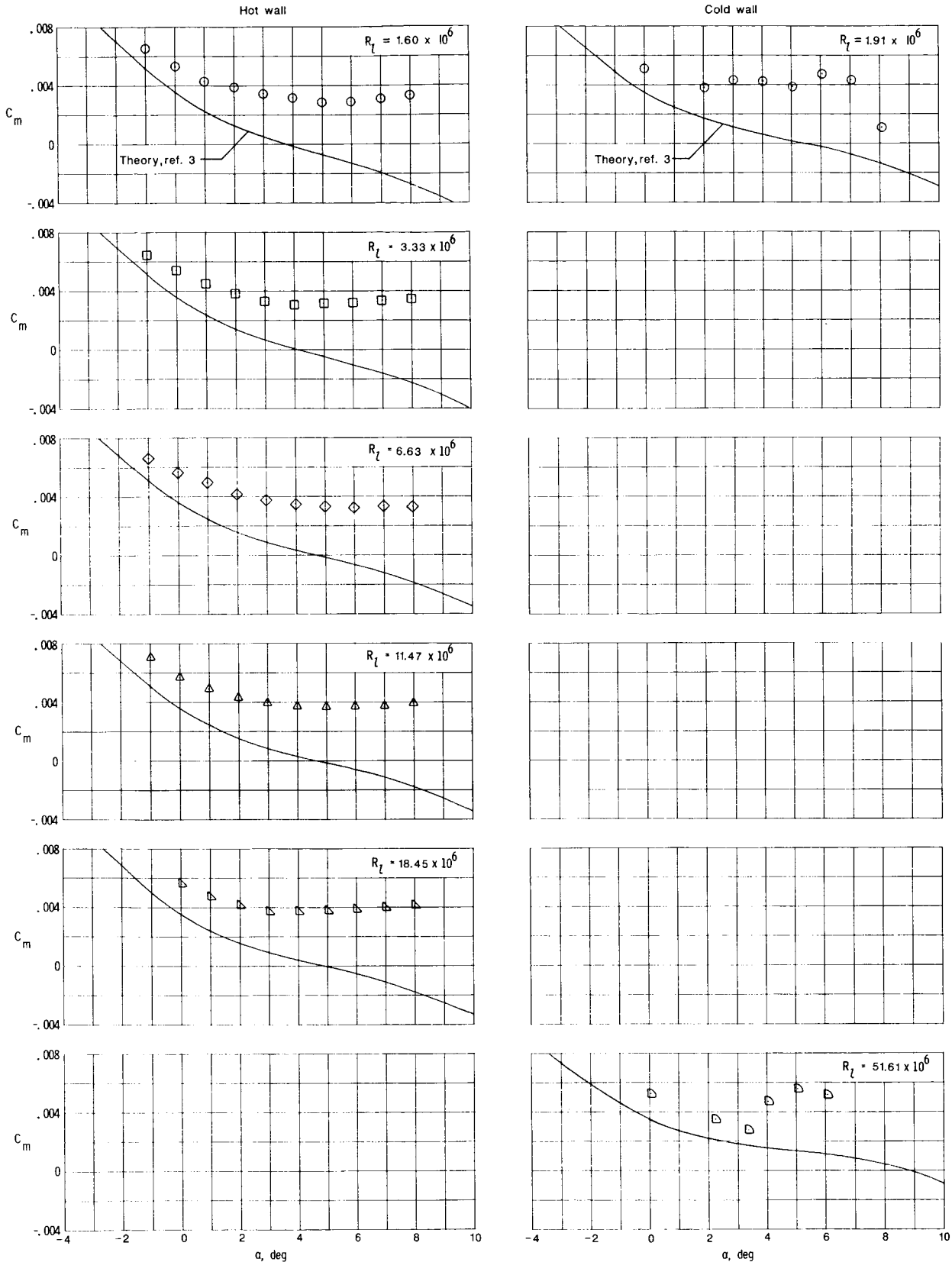

(f) Pitching moment.

Figure 4. Concluded.

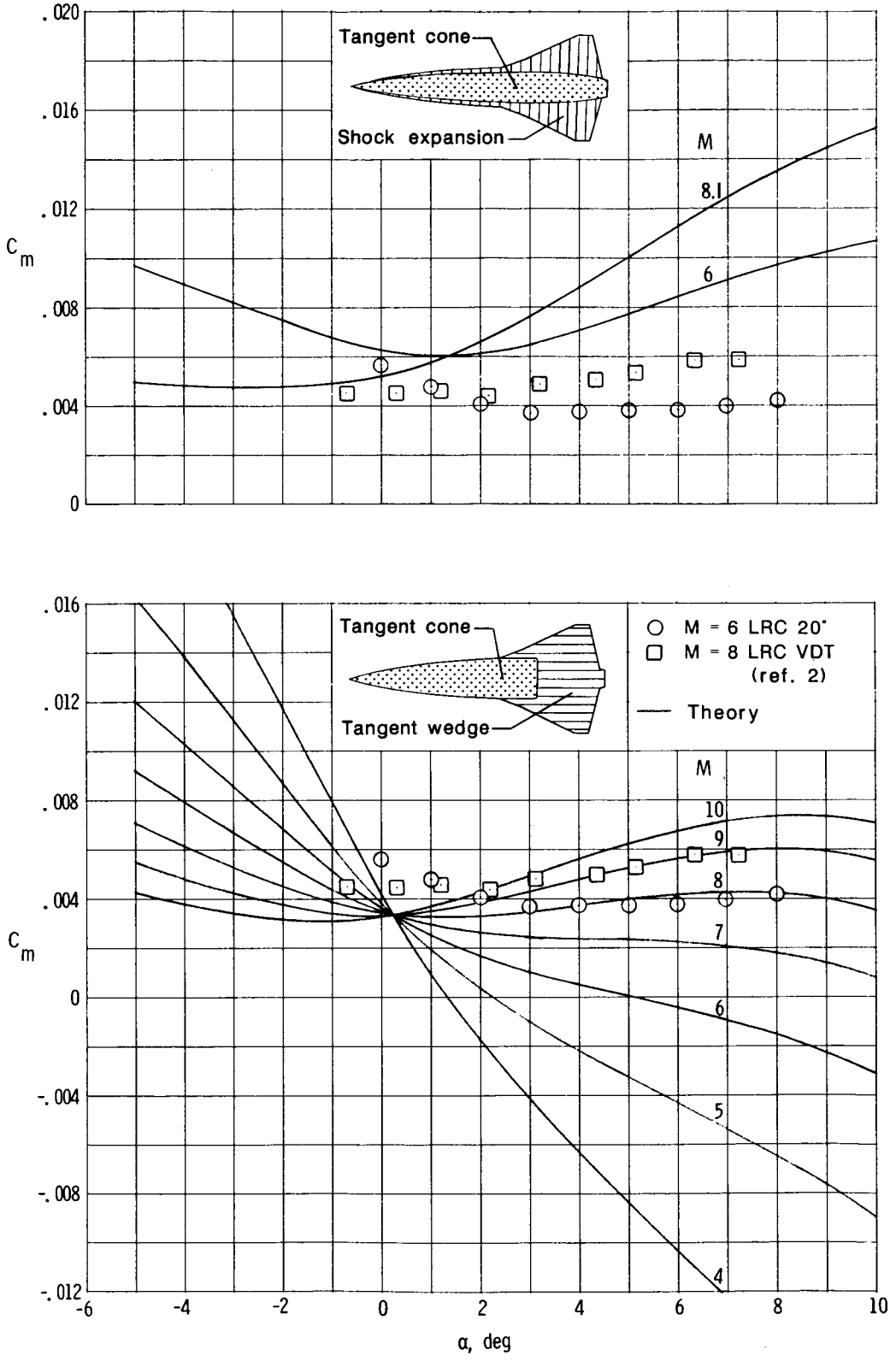

Figure 5. Comparison of experimental pitching moments with estimates from GHABAP using different pressure distribution methods.

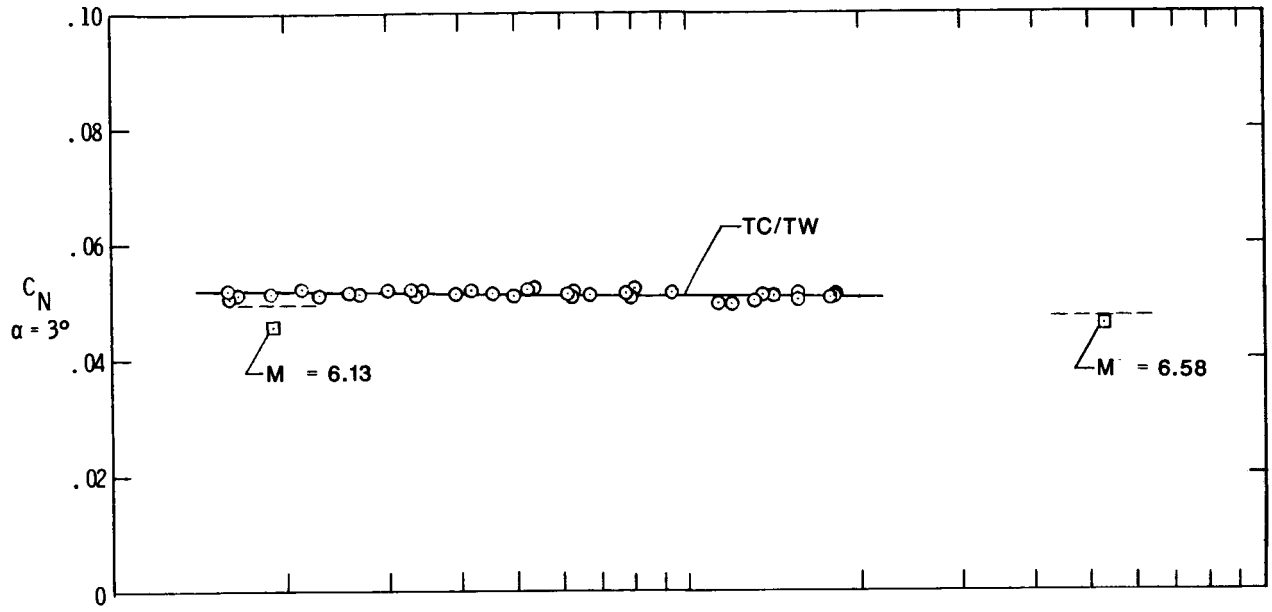

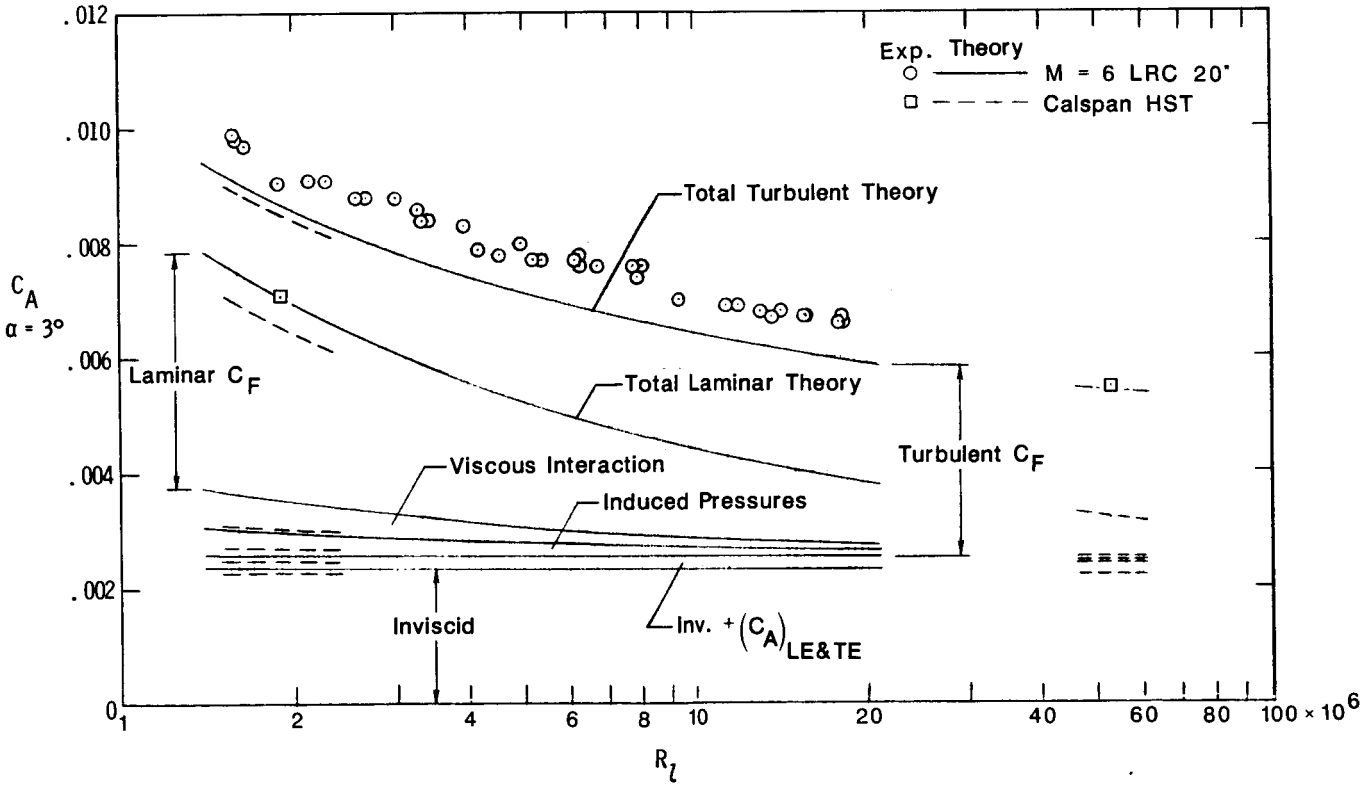

Figure 6. Comparison of experimental normal- and axial-force coefficients with calculations from GHABAP on blended wing-body configuration. $\alpha = 3°$; $M \approx 6$.

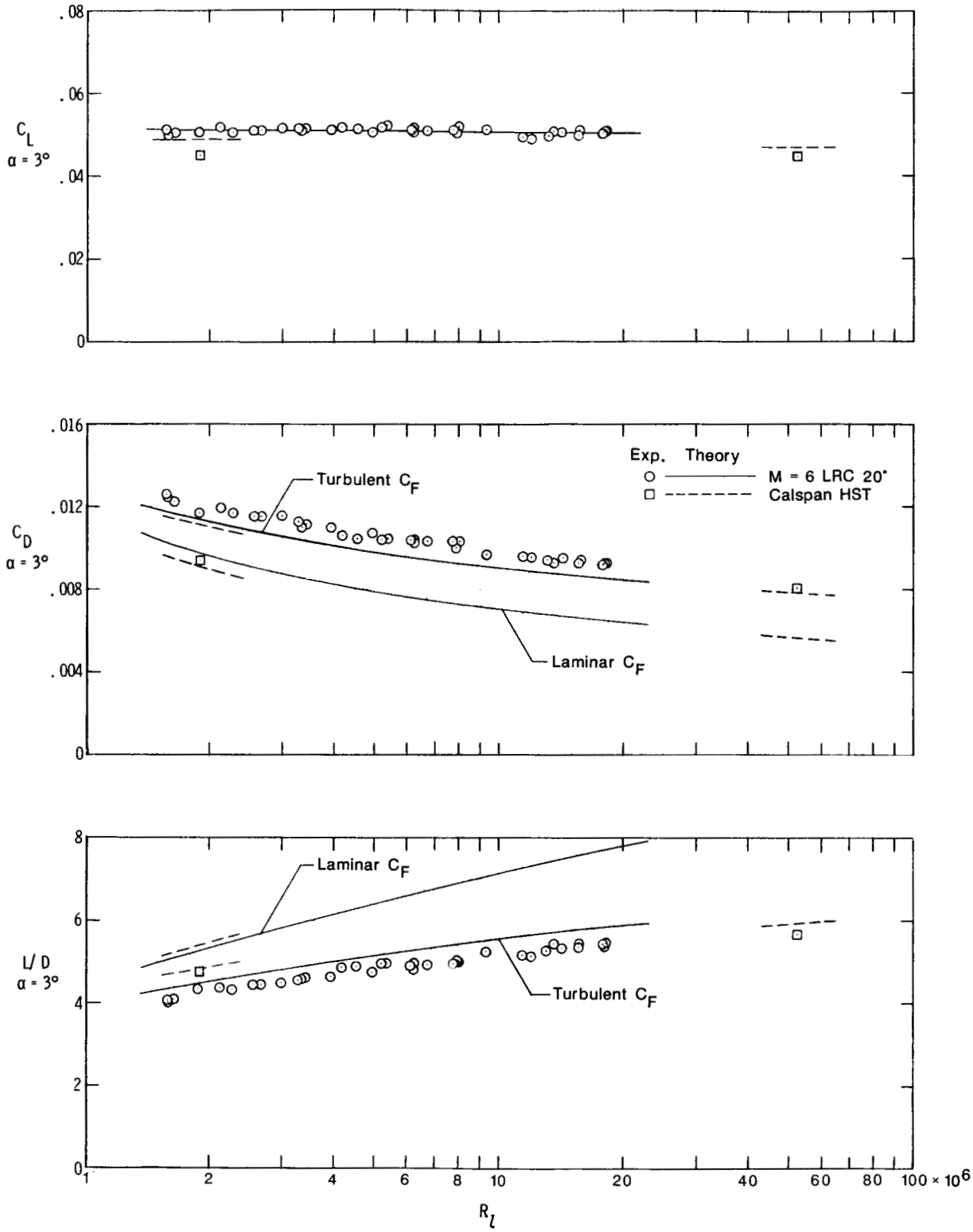

Figure 7. Comparison of experimental lift, drag, and lift-drag ratio with calculations from GHABAP. $\alpha = 3°$; $M \approx 6$.

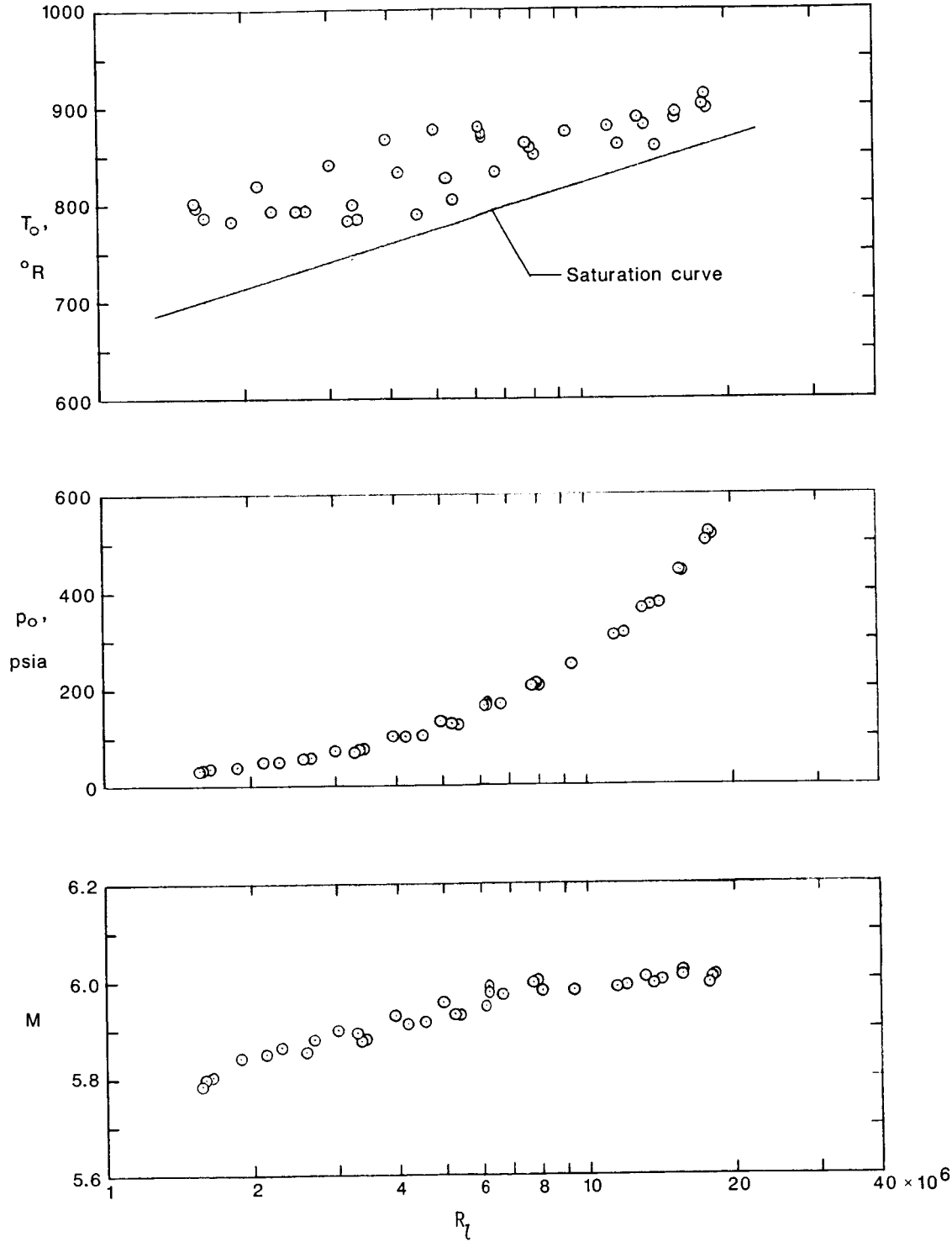

Figure 8. Stagnation conditions and resulting Mach and Reynolds numbers from present tests at $\alpha = 3°$ in Langley 20-Inch Mach 6 Tunnel.

NASA
National Aeronautics and Space Administration

Report Documentation Page

1. Report No.	2. Government Accession No.	3. Recipient's Catalog No.
NASA TP-2728		

4. Title and Subtitle	5. Report Date
Effect of Reynolds Number Variation on Aerodynamics of a Hydrogen-Fueled Transport Concept at Mach 6	August 1987
	6. Performing Organization Code
7. Author(s)	8. Performing Organization Report No.
Jim A. Penland and Don C. Marcum, Jr.	L-16286
9. Performing Organization Name and Address	10. Work Unit No.
NASA Langley Research Center Hampton, VA 23665-5225	505-62-81-01
	11. Contract or Grant No.
12. Sponsoring Agency Name and Address	13. Type of Report and Period Covered
National Aeronautics and Space Administration Washington, DC 20546-0001	Technical Paper
	14. Sponsoring Agency Code

15. Supplementary Notes

16. Abstract

Two separate tests have been made on the same blended wing-body hydrogen-fueled transport model at a Mach number of about 6 and a range of Reynolds number (based on theoretical body length) of 1.577×10^6 to about 55.36×10^6. The results of these tests, made in a conventional hypersonic blowdown tunnel and a hypersonic shock tunnel, are presented through range of angle of attack from $-1°$ to $8°$, with an extended study at a constant angle of attack of $3°$. The model boundary-layer flow appeared to be predominantly turbulent except for the low Reynolds number shock tunnel tests. Model wall temperatures varied considerably between the two tests; the blowdown tunnel varied from about 255°F to 340°F, whereas the shock tunnel had a constant 70°F model wall temperature. The experimental normal-force coefficients were essentially independent of Reynolds number. A current theoretical computer program was used to study the effect of Reynolds number. Theoretical predictions of normal-force coefficients were good, particularly at anticipated cruise angles of attack, that is, $2°$ to $5°$. Axial-force coefficients were generally underestimated for the turbulent skin friction conditions, and pitching-moment coefficients could not be predicted reliably.

17. Key Words (Suggested by Authors(s))	18. Distribution Statement
Hypersonic aircraft Turbulent skin friction Reynolds number effects Computational aerodynamics	Unclassified—Unlimited Subject Category 02

19. Security Classif.(of this report)	20. Security Classif.(of this page)	21. No. of Pages	22. Price
Unclassified	Unclassified	26	A03

NASA FORM 1626 OCT 86

NASA-Langley, 1987

For sale by the National Technical Information Service, Springfield, Virginia 22161-2171